Indian Journal of Chemistry
Vol. 61, January 2022, pp. 69-80

X-ray crystal structure, NMR, DFT investigations, pharmaco-kinetic, and toxicity of sarcotrocheliol: A pyrane-based cemranoids of marine origin

Mohamed E El-Hefnawy[a,c], Jamal Lasri[a], Zahraa A Alsaihati[b], Khalid O Al-Footy[b], Mostafa A Hussien[b,d]& Ali I Ismail*[e]

[a] Department of Chemistry, Rabigh College of Arts and Sciences, King Abdulaziz University, Jeddah, Saudi Arabia

[b] Department of Chemistry, Faculty of Science, Tanta University, Tanta 31527, Egypt

[c] Department of Chemistry, Faculty of Science, King Abdulaziz University, P.O. Box 80203, Jeddah 21589, Saudi Arabia

[d] Department of Chemistry, Faculty of Science, Port Said University, Port Said, 42521, Egypt

[e] Department of Chemistry, Faculty of Science, The Hashemite University, P.O. Box 150459, Zarqa 13115, Jordan

E-mail: aeyesmaeel@kau.edu.sa

Received 18 April 2020; accepted (revised) 26 October 2021

One of a recently discovered marine origin cembranoids has been studied experimentally and theoretically to obtain its thorough structural, electronic, spectroscopic, and biochemical activity. The exact molecular structure of sarcotrocheliol ($C_{20}H_{34}O_2$) **1** has been determined for the first time using a single crystal X-ray diffraction analysis. Crystallography shows that the molecule is crystalline as an orthorhombic, space group of $P2_12_12_1$, with a = 9.20(4) Å, b = 10.80(4) Å, c = 19.99(9) Å. ^{1}H, ^{13}C and DEPT-135 NMR measurements of sarcotrocheliol**1**have been measured in four different deuterated solvents: $CDCl_3$, CD_3CN, MeOH-d_4 and DMSO-d_6. Theoretical calculations have been performed to find the main structural and electronic properties of the compound and matched with the experimental properties. The density functional theory (DFT) method at B3LYP/6-311++G(d,p) level of theory has been used for all computed properties. Vibrational frequencies have been determined using DFT calculations and compared with the experimental values. Computed chemical shifts in the NMR have been determined by the GIAO method. The correlation coefficients between the calculated and experimental NMR chemical shifts have been found to be 0.92 and 0.998 for ^{1}H and ^{13}C NMR, respectively. Physicochemical parameters of the compound *versus* reference drugs have been done. The isolated compound meets the main criteria of the employed rules indicating a drug-like character. The molecular docking studies have been performed for the compound toward the breast and prostate cancers.

Keywords:Sarcotrocheliol, cembranoids, NMR, DFT, B3LYP, single crystal X-ray

Cembranoids have a 14-membered ring (cembrane) that are class of diterpenoids with few numbers of methyl groups and double bonds[1]. Hundreds of cembranoids that are naturally occurring are already reported in the literature. The natural sources of cembranoids are varied from plants to insects to marine coral[2,3]. The compounds in this class, mostly metabolites, involved in many enzymatic processes including oxidation, photochemical ring reduction, and *trans*-annular-cyclization. Cembranoids were the center of many studies that predicted their anticancer, antimicrobial, and anti-inflammatory activities[4-9].

A recently extracted and reported rare pyrane-based cembranoid, sarcotrocheliol, was separated from the soft coral*Sarcophytontrocheliophorum* from the red sea, Saudi Arabia[10].Despite its importance and rareness, the previous study[10] relied only on IR and NMR spectroscopy to solve the structure of the molecule. The purpose of this work is to provide a thorough study of the electronic and structural properties of the sarcotrocheliolemploying a combinedexperimental and computationalapproach. Single crystal X-ray diffraction analysed the crystal and molecular structure of a pure sarcotrocheliol 1 crystal. Moreover, Experimental and theoretical measurements ^{1}H, ^{13}C and DEPT-135 NMR spectra of 1 were carried out in four different deuterated solvents; $CDCl_3$, CD_3CN, MeOH-d_4 and DMSO-d_6. DFT theoretical computations were made to obtain the main structural, electronic and vibrational properties and then compared with the experimental properties. The molecular docking study was performed for compound **1** toward the breast and prostate cancers.

Experimental Section

General experimental details for NMR study

^{1}H, ^{13}C and DEPT-135 NMR spectra of sarcotrocheliol**1** (Figure 1) (in $CDCl_3$, CD_3CN, MeOH-d_4 or DMSO-d_6) were recorded using a Bruker

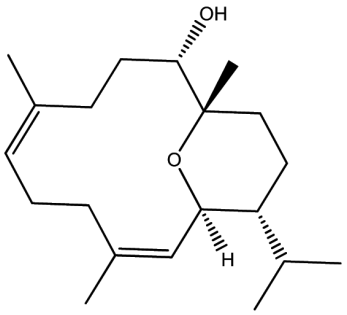

Figure 1 — The sarcotrocheliol molecule **1** with IUPAC name of (1S,2S,5*Z*,9*Z*,11S,12R)-12-isopropyl-1,5,9-trimethyl-15-oxabicyclo [9.3.1]pentadeca-5,9-dien-2-ol

Avance III HD 600 MHz (Ascend^{TM} Magnet) spectrometer at ambient temperature. All chemical shifts (δ) are shown, relative to TMS, in ppm.

Study of ^{1}H,^{13}C and DEPT-135 NMR spectra of sarcotrocheliol 1 in different solvents

^{1}H,^{13}C and DEPT-135 NMR spectra of sarcotrocheliol in $CDCl_3$

^{1}H NMR ($CDCl_3$, 600 MHz): δ 0.74 (d, J_{HH} = 6.6 Hz, 3H, CH_3-16), 0.89 (d, J_{HH} = 6.6 Hz, 3H, CH_3-17), 1.04 (s, 3H, CH_3-20), 1.20 (m, 1H, C*H*-14), 1.27 (m, 1H, C*H*-1), 1.28-1.37 (m, 2H, C*H*-10 and C*H*-15), 1.41-1.48 (m, 2H, CH_2-13), 1.63 (s, 3H, CH_3-19), 1.66 (s, 3H, CH_3-18), 1.78 (t, J_{HH} = 12.9 Hz, 1H, C*H*-10), 1.97-2.04 (m, 2H, C*H*-5 and C*H*-9), 2.14 (t, J_{HH} = 6.6 Hz, 1H, C*H*-9), 2.16-2.21 (m, 2H, C*H*-6 and C*H*-5), 2.31-2.37 (m, 1H, C*H*-6), 2.40 (dt, J_{HH} = 3.4 Hz, 1H, C*H*-14), 3.88 (d, J_{HH} = 9.5 Hz, 1H, C*H*-11), 4.55 (dd, J_{HH} = 10.4, 4.9 Hz, 1H, C*H*-2), 5.00 (dd, J_{HH} = 10.4, 4.9 Hz, 1H, C*H*-7), 5.28 (d, J_{HH} = 10.4 Hz, 1H, C*H*-3). ^{13}C NMR ($CDCl_3$, 150 MHz): δ 15.1 (*C*H_3, *C*-18), 17.3 (*C*H_3, *C*-19), 18.7 (*C*H_2, *C*-13), 20.3 (*C*H_3, *C*-16), 20.8 (*C*H_3, *C*-17), 24.2 (*C*H_3, *C*-20), 25.2 (*C*H_2, *C*-6), 29.0 (*C*H, *C*-15), 31.9 (*C*H_2, *C*-10), 33.7 (*C*H_2, *C*-14), 35.3 (*C*H_2, *C*-9), 39.9 (*C*H_2, *C*-5), 46.6 (*C*H, *C*-1), 71.1 (*C*H, *C*-11), 71.9 (*C*H, *C*-2), 75.0 (*C*, *C*-12), 124.1 (*C*H, *C*-7), 125.5 (*C*H, *C*-3), 136.0 (*C*, *C*-8), 138.7 (*C*, *C*-4). DEPT-135 NMR ($CDCl_3$, 150 MHz): δ 15.1 (*C*H_3, *C*-18), 17.3 (*C*H_3, *C*-19), 18.7 (*C*H_2, *C*-13), 20.3 (*C*H_3, *C*-16), 20.8 (*C*H_3, *C*-17), 24.2 (*C*H_3, *C*-20), 25.2 (*C*H_2, *C*-6), 29.0 (*C*H, *C*-15), 31.9 (*C*H_2, *C*-10), 33.7 (*C*H_2, *C*-14), 35.3 (*C*H_2, *C*-9), 39.9 (*C*H_2, *C*-5), 46.6 (*C*H, *C*-1), 71.1 (*C*H, *C*-11), 71.9 (*C*H, *C*-2), 124.1 (*C*H, *C*-7), 125.5 (*C*H, *C*-3).

^{1}H,^{13}C and DEPT-135 NMR spectra of sarcotrocheliol in CD_3CN

^{1}H NMR (CD_3CN, 600 MHz): δ 0.75 (d, J_{HH} = 6.4 Hz, 3H, CH_3-16), 0.90 (d, J_{HH} = 6.4 Hz, 3H, CH_3-17), 0.93 (s, 3H, CH_3-20), 1.17 (m, 1H, C*H*-14), 1.26 (m, 1H, C*H*-1), 1.27-1.30 (m, 2H, C*H*-10 and C*H*-15), 1.43-1.51 (m, 2H, CH_2-13), 1.62 (s, 3H, CH_3-19), 1.63 (s, 3H, CH_3-18), 1.96-1.98 (m, 2H, C*H*-10 and C*H*-5), 2.05-2.12 (m, 3H, CH_2-9 and C*H*-6), 2.16-2.18 (m, 1H, C*H*-5), 2.33-2.40 (m, 2H, C*H*-6 and C*H*-14), 2.70 (bs, 1H, O*H*), 3.76 (d, J_{HH} = 9.6 Hz, 1H, C*H*-11), 4.45 (dd, J_{HH} = 10.4, 4.9 Hz, 1H, C*H*-2), 5.01 (dd, J_{HH} = 10.4, 4.9 Hz, 1H, C*H*-7), 5.36 (d, J_{HH} = 10.4 Hz, 1H, C*H*-3). ^{13}C NMR (CD_3CN, 150 MHz): δ 14.2 (*C*H_3, *C*-18), 16.7 (*C*H_3, *C*-19), 18.5 (*C*H_2, *C*-13), 19.6 (*C*H_3, *C*-16), 20.1 (*C*H_3, *C*-17), 23.8 (*C*H_3, *C*-20), 24.8 (*C*H_2, *C*-6), 28.9 (*C*H, *C*-15), 31.3 (*C*H_2, *C*-10), 33.7 (*C*H_2, *C*-14), 34.9 (*C*H_2, *C*-9), 39.4 (*C*H_2, *C*-5), 46.7 (*C*H, *C*-1), 70.3 (*C*H, *C*-11), 70.8 (*C*H, *C*-2), 75.0 (*C*, *C*-12), 123.7 (*C*H, *C*-7), 126.0 (*C*H, *C*-3), 136.1 (*C*, *C*-8), 137.9 (*C*, *C*-4). DEPT-135 NMR (CD_3CN, 150 MHz): δ 14.2 (*C*H_3, *C*-18), 16.7 (*C*H_3, *C*-19), 18.5 (*C*H_2, *C*-13), 19.6 (*C*H_3, *C*-16), 20.1 (*C*H_3, *C*-17), 23.8 (*C*H_3, *C*-20), 24.8 (*C*H_2, *C*-6), 28.9 (*C*H, *C*-15), 31.3 (*C*H_2, *C*-10), 33.7 (*C*H_2, *C*-14), 34.9 (*C*H_2, *C*-9), 39.4 (*C*H_2, *C*-5), 46.7 (*C*H, *C*-1), 70.3 (*C*H, *C*-11), 70.8 (*C*H, *C*-2), 123.7 (*C*H, *C*-7), 126.0 (*C*H, *C*-3).

^{1}H,^{13}C and DEPT-135 NMR spectra of sarcotrocheliol in MeOH-d_4

^{1}H NMR (MeOH-d_4, 600 MHz): δ 0.76 (d, J_{HH} = 6.4 Hz, 3H, CH_3-16), 0.92 (d, J_{HH} = 6.4 Hz, 3H, CH_3-17), 1.02 (s, 3H, CH_3-20), 1.23-1.56 (m, 6H, C*H*-14, C*H*-1, C*H*-10, C*H*-15 and CH_2-13), 1.64 (s, 3H, CH_3-19), 1.68 (s, 3H, CH_3-18), 2.03-2.15 (m, 5H, C*H*-10, C*H*-5, CH_2-9 and C*H*-6), 2.21-2.23 (m, 1H, C*H*-5), 2.36-2.41 (m, 1H, C*H*-6), 2.44-2.46 (m, 1H, C*H*-14), 3.85 (d, J_{HH} = 9.8 Hz, 1H, C*H*-11), 4.53 (dd, J_{HH} = 10.4, 4.9 Hz, 1H, C*H*-2), 5.02 (dd, J_{HH} = 10.4, 4.9 Hz, 1H, C*H*-7), 5.37 (d, J_{HH} = 10.4 Hz, 1H, C*H*-3). ^{13}C NMR (MeOH-d_4, 150 MHz): δ 13.9 (*C*H_3, *C*-18), 16.2 (*C*H_3, *C*-19), 18.3 (*C*H_2, *C*-13), 19.3 (*C*H_3, *C*-16), 19.7 (*C*H_3, *C*-17), 23.3 (*C*H_3, *C*-20), 24.7 (*C*H_2, *C*-6), 28.9 (*C*H, *C*-15), 30.7 (*C*H_2, *C*-10), 33.6 (*C*H_2, *C*-14), 34.8 (*C*H_2, *C*-9), 39.4 (*C*H_2, *C*-5), 46.7 (*C*H, *C*-1), 70.5 (*C*H, *C*-11), 71.0 (*C*H, *C*-2), 75.9 (*C*, *C*-12), 123.7 (*C*H, *C*-7), 125.0 (*C*H, *C*-3), 135.8 (*C*, *C*-8), 139.0 (*C*, *C*-4). DEPT-135 NMR (MeOH-d_4, 150 MHz): δ 13.9 (*C*H_3, *C*-18), 16.2 (*C*H_3, *C*-19), 18.3 (*C*H_2, *C*-13), 19.3 (*C*H_3, *C*-16), 19.7 (*C*H_3, *C*-17), 23.3 (*C*H_3, *C*-20), 24.7 (*C*H_2, *C*-6), 28.9 (*C*H, *C*-15),

30.7 (*C*H_2, *C*-10), 33.6 (*C*H_2, *C*-14), 34.8 (*C*H_2, *C*-9), 39.4 (*C*H_2, *C*-5), 46.7 (*C*H, *C*-1), 70.5 (*C*H, *C*-11), 71.0 (*C*H, *C*-2), 123.7 (*C*H, *C*-7), 125.0 (*C*H, *C*-3).

^{1}H,^{13}C and DEPT-135 NMR spectra of sarcotrocheliol in DMS0-d_6

^{1}H NMR (DMSO-d_6, 600 MHz): δ 0.69 (d, J_{HH} = 6.3 Hz, 3H, CH_3-16), 0.84 (d, J_{HH} = 6.3 Hz, 3H, CH_3-17), 0.87 (s, 3H, CH_3-20), 1.04-1.24 (m, 3H, C*H*-14, C*H*-1, C*H*-10), 1.36-1.42 (m, 1H, C*H*-15), 1.48-1.53 (m, 2H, CH_2-13), 1.55 (s, 3H, CH_3-19), 1.57 (s, 3H, CH_3-18), 1.94-1.96 (m, 4H, C*H*-10, C*H*-5, CH_2-9), 2.03-2.06 (m, 1H, C*H*-6), 2.12-2.14 (m, 1H, C*H*-5), 2.23-2.30 (m, 1H, C*H*-6), 2.35-2.38 (m, 1H, C*H*-14), 3.60 (dd, J_{HH} = 9.4, 6.9 Hz, 1H, C*H*-11), 4.35 (dd, J_{HH} = 10.4, 4.7 Hz, 1H, C*H*-2), 4.45 (d, J_{HH} = 6.9, 1H, O*H*), 4.92 (dd, J_{HH} = 10.0, 4.9 Hz, 1H, C*H*-7), 5.25 (d, J_{HH} = 10.4 Hz, 1H, C*H*-3). ^{13}C NMR (DMSO-d_6, 150 MHz): δ 15.1 (*C*H_3, *C*-18), 17.7 (*C*H_3, *C*-19), 18.8 (*C*H_2, *C*-13), 20.6 (*C*H_3, *C*-16), 21.1 (*C*H_3, *C*-17), 24.9 (*C*H_3, *C*-20), 25.2 (*C*H_2, *C*-6), 29.1 (*C*H, *C*-15), 31.4 (*C*H_2, *C*-10), 34.0 (*C*H_2, *C*-14), 35.3 (*C*H_2, *C*-9), 39.9 (*C*H_2, *C*-5), 46.6 (*C*H, *C*-1), 70.0 (*C*H, *C*-11), 70.3 (*C*H, *C*-2), 75.4 (*C*, *C*-12), 123.7 (*C*H, *C*-7), 126.2 (*C*H, *C*-3), 136.2 (*C*, *C*-8), 137.5 (*C*, *C*-4). DEPT-135 NMR (DMSO-d_6, 150 MHz): δ 15.1 (*C*H_3, *C*-18), 17.7 (*C*H_3, *C*-19), 18.8 (*C*H_2, *C*-13), 20.6 (*C*H_3, *C*-16), 21.1 (*C*H_3, *C*-17), 24.9 (*C*H_3, *C*-20), 25.2 (*C*H_2, *C*-6), 29.1 (*C*H, *C*-15), 31.4 (*C*H_2, *C*-10), 34.0 (*C*H_2, *C*-14), 35.3 (*C*H_2, *C*-9), 39.9 (*C*H_2, *C*-5), 46.6 (*C*H, *C*-1), 70.0 (*C*H, *C*-11), 70.3 (*C*H, *C*-2), 123.7 (*C*H, *C*-7), 126.2 (*C*H, *C*-3).

X-ray crystallography

Bruker AXS-KAPPA APEX II diffractometer instrument based on graphite monochromatedCuKa radiation was used to determine X-ray structure. The compound was extracted from *soft coral S. trocheliophorum* using 1:1 chloroform/methanol solution as explained by Alarif *et al*.[10] The crystal was obtained by slow evaporation from spectroscopy grade chloroform solvent. A good quality crystal is installed on the rod of the goniometer under inert gas (nitrogen gas). The collection of the diffraction data was performed at 0.46 per frame omega scans at 293 K. The softwares Bruker-SMART software and Bruker-SAINT were used to save and refine the cell parameters, respectively. The structure was solved and visualized by the SHELXS-97[11,12] and MERCURY[13], respectively. The relevant crystallographic information is provided in Table I. For this work the file "CCDC 1535957" (www.ccdc.cam.ac.uk/data request / cif) has the supplementary crystallographic data.

Computational methods

Density functional theory (DFT) was utilized to obtain the molecular, structural, electronic, and vibrational characteristics of the title compound. The calculations were completed by DFT and Time Based DFT (TD-DFT). The DFT calculations were done using a hybrid function of Becke's three-parameter exchange with Lee–Yang–Parr (LYP) correlation functional. Gaussian 09 software[14] was used to determine the full geometry optimization of sarcotrocheliol**1** at the B3LYP level of theory using a triple-zeta diffuse basis sets 6-311G++(d,p) in gas phase and in different solvents using PCM model

Table I — Crystallographic information of sarcotrocheliol**1** and precision of the structure as determined by single crystal X-ray measurements

Formula	$C_{20}H_{34}O_2$
Fw	306.5
T (K)	293(1)
Crystal system	Orthorhombic
Space group	P 2_1 2_1 2_1
a (Å)	9.20(4)
b (Å)	10.80(4)
c (Å)	19.99(9)
α (°)	90
β (°)	90
γ (°)	90
V (nm^3)	1986.21
Z	4
density ($mg.cm^{-3}$)	1.024
F(000)	680
Crystal dimensions (mm)	0.08 × 0.2 × 0.4
θ range (°)	2.9, 27.1
hkl ranges	−10< h < 10
	−12< k < 12
	−23 < l < 23
Data/parameters	3513, 208
Goodness-of-fit	0.992
Final R indices [I > 2σ (I)]	R1 = 0.0687
	wR2 = 0.1351
Highest peak/ deepest hole	Δρmax = 0.161 $eÅ^{-3}$ / Δρmin = −0.136 $eÅ^{-3}$

(Polarizable Continuum Model). The absence of negative frequency is used as an important parameter for verifying the optimization. UV–Vis electronic absorption (TD method) and NMR chemical shifts (GIAO method) were determined using the final optimized geometries at the high level of theory, B3LYP/6-311G++(d,p) in gas phase and different solvents. The softwares; Chemcraft[15], GaussSum[16] and Veda 4[17] were used to analyze the Gaussian 09 output files.

Protein Analysis

The bioactivity score and physicochemical properties of the compound were calculated by Molinspiration 2016.03 whereas the toxicity was determined by OSIRIS data warrior 4.6.1[18]. The structures of receptors middle domain of HSP90 for breast cancer (PDB i.d. 1HK7)[19] and the androgen receptor pf H874Y for prostate cancer mutant (PDB i.d. 2qk7)[20] were downloaded from protein data bank (http://www.rcsb.org/pdb/home/home.do). All docking studies were performed by the MOE software. The compound and the two cancer proteins were compiled using ChemBioDraw ultra. 3D structures were created using ChemBio3D ultra 13.0 software. After that MOPAC software was used to find optimized geometry. For the generation of ligand and enzyme structures; all water molecules in the downloaded proteins and cofactors were removed then the hydrogen atoms were inserted following the preparation of the two proteins. MMFF94x force field was used to specify the parameters and charges. The site-finder module of MOE created the alpha-site spheres after the structural model of complexes was docked on the surface of the minor groove's interior using MOE's DOCK module[21-24]. The Dock scoring was performed utilizing London dG scoring function in MOE software and was enhanced by two different methods of refinement. Auto-rotatable bonds were allowed; evaluating the best ten binding poses was guided to achieve the best score. The docking pose database browser was used to compare the docking poses in the co-crystallized structure with the ligand, and to obtain a pose of RMSD. The sorting criteria were the binding affinity of sarcotrocheliol**1** with the protein, the binding free energy, the hydrogen bonds between the compound and amino acid in the receptor, and the RMSD of the compound position compared to the docking pose. Hydrogen bonds were considered only if the hydrogen bond length is less or equal to 3.5 A°. Both RMSD and the mode of interaction of the protein ligand were used as standard docked models.

The PreADMET program was accessed from http://preadmet.bmdrc.org/. Andrographolide and eight structure modifications were used in this study (Figure 1). The structure of all compounds was transferred into molfile (*.mol). The program calculated the predictive absorption for Caco-2 cell, human intestinal absorption (HIA), and plasma protein binding. Estimating the toxicity properties (mutagenicity and carcinogenicity) was achieved using Toxtree software and Benigni/Bossa rule-base methods.

Results and Discussion

NMR study of sarcotrocheliol 1 in different solvents

The spectra of sarcotrocheliol 1 ^{1}H, ^{13}C, and DEPT-135 NMR were examined in four different solvents. In the ^{1}H NMR spectra, there was a small variation in the chemical shifts when using CD_3CN, MeOH-d_4 or DMSO-d_6 instead of $CDCl_3$. For example, comparing the chemical shifts of the protons *H*-11 and *H*-2 which are situated near the electronegative oxygen atom, it was observed that proton *H*-11 appears at δ 3.88, 3.76, 3.85 and 3.60, and, *H*-2 proton was detected at δ 4.55, 4.45, 4.53 and 4.35 in $CDCl_3$, CD_3CN, MeOH-d_4 and DMSO-d_6, respectively (see Experimental Section and also the ^{1}H NMR spectra on the Supplementary Information). On the other hand, the alcohol proton O*H* was not observed in the case of $CDCl_3$. However, in CD_3CN, the alcohol proton O*H* was observed as a broad signal at δ 2.70. In DMSO-d_6, the O*H* proton was detected as a doublet at δ 4.45 with coupling constant J_{HH} = 6.9 Hz. This behavior, which was only observed in DMSO-d_6, can be explained due to the coupling of O*H* proton with the adjacent proton *H*-11. In MeOH-d_4, the alcohol proton O*H* was not observed because of the rapid exchange with the solvent or the water in the solvent.

In the ^{13}C NMR spectra, it was observed that the carbons *C*-2 and *C*-12 directly attached to the oxygen atom (or *C*-11 attached to *O*H) were slightly affected by the solvent. For example, *C*-11 was detected at δ 71.1, 70.3, 70.5 and 70.0 in $CDCl_3$, CD_3CN, MeOH-d_4 and DMSO-d_6, respectively. On the other hand, the chemical shifts (in $CDCl_3$) at δ 136.0 and 138.7 shows that *C*-8 and *C*-4, respectively, are olefinic carbon atoms. In the DEPT-135 NMR spectra, the signals of *C*-4, *C*-8 and *C*-12 are absent which indicates that they are quaternary carbon atoms.

Crystal structure determination

The molecular structure and atoms numbering of sarcotrocheliol**1** are presented in Figure 2. Also, the crystal packing along the *a*-axis is shown in Figure 3.

Table I displays the crystal data and compound 1 structure refinement. Table S1 (Supplementary Information) lists specific parameters of crystals; bond lengths, bond angles, and angles of torsion. Sarcotrocheliol**1** is found to be crystallized in the $P2_12_12_1$ space group containing four molecules per cell unit. The compound shows the main cembranoid skeleton which is the 14-membered ring with few double bonds and methyl-group branches. However, **1** is composed of a rare pyran-based structure that is formed from connecting oxygen atom with two carbon atoms. The resulting structure is oxabicyclic that has two cycles that are fused at C2-O1-C12; six-membered ring (tetrahydropyran) and twelve-membered ring with two non-conjugated double bonds (oxacyclododecadiene). The final structure has three methyl, one isopropyl, and one hydroxyl groups. The six-membered ring has a near chair configuration with isopropyl group branching from C1 at the equatorial position. However, two angles appear to be stretched, compared to the perfect chair configuration, C2-O1-C12 (120.0º) and C1-C13-C14 (115.7º) which might be due to the existence of; the larger ring, the oxygen atom and the isopropyl group. The 12-memebered structure has two double bonds that provide a relatively constrained configuration. Most angles are found to be within the expected values except two vinylene angles; C2-C3-C4 and C8-C7-C6 which are found to be particularly high with a value of more than 127º which may result from the constraint of the 12-memebered ring. C2-C3 and C8-C7 are determined to be double bonds based on their bond lengths; 1.350 and 1.34 Å, respectively. Also, C-H bond length of the vinyl groups is found to be 0.931 Å and 0.93 Å for C3-H3 and C7-H7, respectively. C-C bond lengths of the rest of carbon atoms are found to be in the range of 1.491-1.564 Å which are the normal values for sp^3 carbon atoms. Also, C-H bond lengths are reported to be 0.96-0.98 Å. In the crystal, the molecules are assumed to be stabilized by O2 ---H21···· O1 intermolecular hydrogen bonds (Table II and Figure 3).

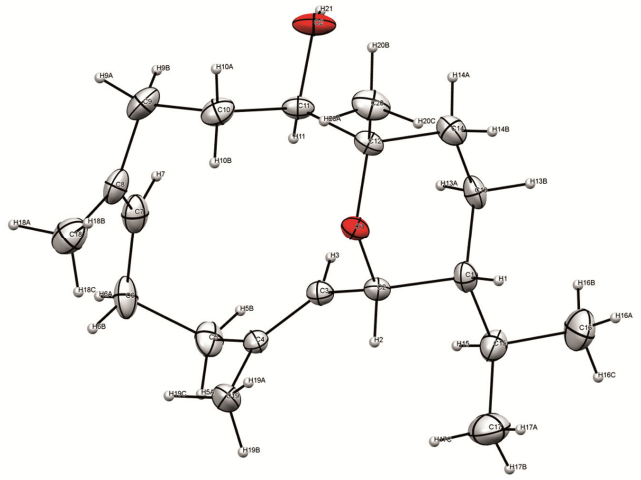

Figure 2 — ORTEP Sarcotrocheliol**1** description focused on the structural data of the crystals; displaying the numbering scheme of atoms and the probability of displacement ellipsoids of non-H atoms by 20%.

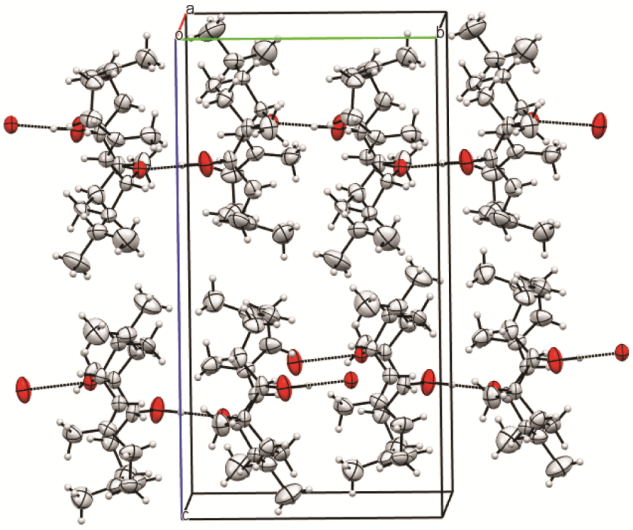

Figure 3 — Packing diagram for sarcotrocheliol**1**, viewed down the *a*-axis, displaying the intermolecular H-bonding as dashed lines

Computational study of the structure 1

Geometry optimization

sarcotrocheliol**1**structure was optimized using DFT at the B3LYP/6-311++G(d,p) level of theory. The HF energy was estimated as -933.27319789 a.u. whereas the calculated dipole moment was 2.1571 D. The detailed bond lengths, bond and torsion angles are presented in Table S1 (Supplementary Information) with the comparison with the experimental data. The theory was able to provide relatively good expectations, *i.e.*, the angles C2-C3-C4 and C8-C7-C6 are found to be as high as the experimental value (above 127º). Also, C2-C3 and C8-C7 are determined to be double bonds due to their bond lengths values; 1.3405 and 1.334 Å, respectively, which are almost as same as the experimental values. C-C bond lengths of

Table II — The possible Hydrogen intermolecular bonds that revealed from crystal packing (Å,°)

D H A	D – H	H...A	D...A	D - H...A
O2 --- H... O1	1.04(3)	1.757(3)	2.797(2)	170(3)

the rest of the carbon atoms are found to be in the range of the experimental values with an error of less than 2%. In general, The geometrical parameters changes between the crystal and the optimized structures are not significant when related to the C-C or C-O bonds. However, all C-H bond lengths are noticed to be mostly overestimated for all H-X bonds (vinyl-C-H, sp^3-C-H, or O-H) which agrees with previous studies[25]. Also, the two angles were found underestimated by more than 5% compared with experimental values; H21-O2-C11 and O1-C2-H2. The correlation coefficient for the bond length, bond angles, and torsion angles between the experimental and theoretical are determined to be 0.9438, 0.8525 and 0.994, respectively, with a slope of 1.00 (the intercept was forced to be 0) for all plots (Fig. S1). (Supplementary Information).

Vibrational and potential energy distribution (PED) analysis

Sarcotrocheliol**1** has 56 atoms, belongs to C1 point group and has 168 normal vibration modes along with the 162 degrees of freedom. The fundamental vibrations of the optimized geometry of the ground state for **1** are assigned at the B3LYP/6-311++G(d,p) level using the Gaussian 09 program. Vibration frequencies computed at B3LYP/6-311G(d,p) level were multiplied by 0.9679 which is a typical scaling factor for this method[26].

The experimental FTIR results reported seven peaks for the IR spectrum at 3470, 3053, 2935, 1661, 1442, 1355 and 860 cm^{-1}as reported by Alarif *et al*.[10]

Two sharp peaks at 3053 and 2935 cm^{-1} that arcoerresponding to the C-H stretching frequencies are calculated at 2971 and 2932 cm^{-1}. The peak that is attributed to C= C stretching at 1661 cm^{-1} is estimated at 1655 cm^{-1} theoretically. Table S2 (Supplementary Information) provided the detailed descriptions of the assignment. The computed frequencies were allocated through the Veda 4 software[17]. The predicted "scaled" vibrational frequencies are harmonious with the experimental data which means that the scaling factor is necessary and working well. However, the stretching frequency of O-H (experimentally 3470 cm^{-1}) is found by DFT at 3728.6 cm^{-1}. This poor correlation between the experimental and calculated value could be attributed to the difficulty in assigning the peak experimentally due to its broadening nature, and the hydrogen bonding effect in DFT.

NMR analysis

The NMR analysis was done by measuring the ^1H, ^{13}C and DEPT-135 NMR spectra for the sarcotrocheliol**1** experimentally in four different deuterated solvents ($CDCl_3$, CD_3CN, MeOH-d_4, and DMSO-d_6). Also, the chemical shifts of ^1H and ^{13}C nuclei were calculated using DFT. A comparison lists of chemical shifts for ^1H and ^{13}C nuclei obtained experimentally and theoretically are shown in Table III with the atom numbering the same as in Figure 2. Chemical shifts in the ^1H and ^{13}C NMR spectra were allocated using DFT calculations of shielding constants which were referenced by TMS shielding constants which were determined at the same theory level. The experimental results were in good agreement with the theoretically calculated chemical shifts by judging the values of the correlation coefficients (the intercept was forced to be 0). R^2 is found to be 0.932 for ^1H using the solvents DMSO-$d_6$and CD_3CN, 0.9261 for MeOH-d_4, and 0.9406 for $CDCl_3$. Besides, the correlation coefficients for ^{13}C are 0.9985 for each of CD_3CN and $CDCl_3$, 0.9989 for DMSO-d_6 and 0.9988 for MeOH-d_4 (Fig. S2) (Supplementary Information).

Electronic spectra

In the calculated UV spectra, TD-DFT with PCM was used for modeling the solvent effect. Four solvents were used for this study; $CHCl_3$, CH_3CN, MeOH, and DMSO. The spectra were also calculated in gas phase for comparison. Three relatively weak absorption wavelengths (λ_{max}) are expected in the UV spectrum based on calculations. The computed λ_{max} and their corresponding oscillator strength are listed in Table IV. The major orbital contribution in the UV spectrum was determined and given in Table IV (column 3). The calculation revealed that the absorption wavelengths were sensitive to the solvent used. In $CHCl_3$, the three λ_{max}'s were shifted from the gas phase to lower values (bathochromic shift). The other three solvents (CH_3CN, MeOH and DMSO) had no significant differences in their electronic results

Table III — The details ^{1}H and ^{13}C chemical shifts of sarcotrocheliol**1** measured experimentally and calculated by (GIAO B3LYP/6-311++G(d,p)) in four different deuterated solvents

Atom	$CDCl_3$		CD_3CN		MeOH-d_4		DMSO-d_6	
	Exp.	DFT	Exp	DFT	Exp.	DFT	Exp.	DFT
C-18	15.1	16.4694	14.2	16.2436	13.9	16.2484	15.1	16.2315
C-19	17.3	15.1908	16.7	14.9913	16.2	14.9946	17.7	14.983
C-13	18.7	21.3813	18.5	21.1834	18.3	21.187	18.8	21.174
C-16	20.3	21.0348	19.6	20.9765	19.3	20.977	20.6	20.9754
C-17	20.8	20.5626	20.1	20.5242	19.7	20.5242	21.1	20.5239
C-20	24.2	24.2627	23.8	24.2492	23.3	24.2492	24.9	24.2492
C-6	25.2	30.3073	24.8	30.2732	24.7	30.2738	25.2	30.2716
C-15	29	33.4405	28.9	33.4658	28.9	33.4651	29.1	33.4676
C-10	31.9	33.4405	31.3	33.6605	30.7	33.6558	31.4	33.6728
C-14	33.7	35.8454	33.7	35.7193	33.6	35.7217	34	35.7132
C-9	35.3	39.613	34.9	39.4171	34.8	39.4213	35.3	39.406
C-5	39.9	44.4018	39.4	43.959	39.4	43.9681	39.9	43.936
C-1	46.6	50.808	46.7	50.7709	46.7	50.7712	46.6	50.7704
C-11	71.1	75.3088	70.3	76.8067	70.5	76.8064	70	76.8074
C-2	71.9	76.7883	70.8	75.8053	71	75.7951	70.3	75.8311
C-12	75	80.9823	75	81.2093	75.9	81.2044	75.4	81.2218
C-7	124.1	130.8794	123.7	131.4879	123.7	131.4743	123.7	131.5234
C-3	125.5	132.252	126	132.2459	125	132.2445	126.2	132.2497
C-8	136	146.702	136.1	146.5811	135.8	146.5844	136.2	146.5717
C-4	138.7	151.1682	137.9	151.059	139	151.0646	137.5	151.046
Atom	$CDCl_3$		CD_3CN		MeOH-d_4		DMSO-d_6	
	Exper.	DFT	Exper.	DFT	Exper.	DFT	Exper.	DFT
C*H*-1	1.27	1.0805	1.26	1.078767	1.23-1.57	1.077133	1.04-1.25	1.082933
CH-2	4.55	4.5183	4.45	4.5473	4.53	4.5469	4.35	4.5484
CH-3	5.28	5.4639	5.36	5.5379	5.37	5.5364	5.25	5.5416
CH_2-5	1.97-2.04	2.2256	1.96-1.98	2.2277	2.03-2.15	2.2278	1.94-1.97	2.20265
	2.16-2.21	2.00686	2.16-2.18	2.079533	2.21-2.23	2.0791	2.12-2.14	2.0612
CH_2-6	2.16-2.21	2.00686	2.33-2.4	2.079533	2.03-2.19	2.0791	2.03-2.06	2.0612
	2.31-2.37	2.5482	2.05-2.14	2.5566	2.36-2.41	2.5565	2.23-2.30	2.5569
CH-7	5.0	5.1335	5.01	5.1898	5.02	5.1885	4.92	5.193
CH_2-9	1.97-2.04	2.00686	2.05-2.13	2.079533	2.03-2.17	2.0791	1.94-1.98	2.0612
	2.14	2.1397		2.079533	2.03-2.18	2.0791	1.94-1.99	2.0612
CH_2-10	1.28-1.37	1.3203	1.27-1.30	1.27454	1.23-1.58	1.274	1.04-1.26	1.27594
	1.78	1.4499	1.96-1.98	1.4325	2.03-2.15	1.4331	1.94-1.96	1.4309
CH-11	3.88	3.9608	3.76	4.015	3.85	4.014	3.6	4.0173
CH_2-13	1.41-1.48	1.232	1.43-1.51	2.079533	1.23-1.61	2.0791	1.48-1.54	2.20265
		1.5312		1.1402		1.1399		1.1407
CH_2-14	1.2	1.0805	1.17	1.27454	1.23-1.56	1.274	1.04-1.24	1.27594
	2.4	2.1397	2.33-2.41	1.53155	2.44-2.46	1.53155	2.35-2.38	1.53165
CH-15	1.28-1.37	1.232	1.27-1.30	1.27454	1.23-1.59	1.274	1.36-1.42	1.27594
CH_3-16	0.74	0.3755	0.75	0.38435	0.76	0.3842	0.69	0.3846
		1.232		1.27454		1.274		1.27594
		0.786		0.7757		0.7756		0.7758
CH_3-17	0.89	0.3026	0.9	0.3081	0.92	0.308	0.84	0.3082
		0.6453		0.6545		0.6543		0.6549
		0.786		0.8833		0.8836		0.8826

(*contd.*)

Table III — The details ^{1}H and ^{13}C chemical shifts of sarcotrocheliol**1** measured experimentally and calculated by (GIAO B3LYP/6-311++G(d,p)) in four different deuterated solvents (*contd.*)

Atom	$CDCl_3$		CD_3CN		MeOH-d_4		DMSO-d_6	
	Exp.	DFT	Exp.	DFT	Exp.	DFT	Exp.	DFT
CH_3-18	1.66	1.5312	1.63	1.53155	1.68	1.53155	1.57	1.53165
		1.5312		1.53155		1.53155		1.53165
		2.00686		2.079533		2.0791		2.0612
CH_3-19	1.63	2.00686	1.62	1.9114	1.64	1.9121	1.55	1.9098
		1.232		1.27454		1.274		1.27594
		1.5312		1.53155		1.53155		1.53165
CH_3-20	1.04	0.8943	0.93	1.0086	1.02	1.009	0.87	1.0077
		1.0805		1.078767		1.077133		1.082933
		0.3755		0.38435		0.3842		0.3846
O-H	-	1.0805	2.7	1.078767	-	1.077133	4.45	1.082933

Table IV — The predicted singlet state transitions of sarcotrocheliol molecule **1**, computed by TD-DFT method, with its oscillator strength and major contribution of orbitals in gas phase and in four different solvents

	Wavelength (nm)	Oscillator Strength	Major orbitals contributions
	228.2100	0.0004	HOMO→LUMO (69%), HOMO→L+1 (18%)
MeOH	222.7008	0.0055	H-1→LUMO (19%), HOMO→LUMO (18%), HOMO→L+1 (44%)
	221.8202	0.0118	H-1→LUMO (66%), HOMO→L+1 (16%), HOMO→L+3 (10%)
	228.1386	0.0005	HOMO→LUMO (69%), HOMO→L+1 (18%)
DMSO	222.6168	0.0053	H-1→ LUMO (16%), HOMO → LUMO (18%), HOMO→L+1 (46%)
	221.7528	0.0132	H-1→LUMO (68%), HOMO→L+1 (14%)
	228.1848	0.0004	HOMO→LUMO (69%), HOMO→L+1 (18%)
CH_3CN	222.6768	0.0054	H-1→LUMO (18%), HOMO→LUMO (18%), HOMO→L+1 (45%)
	221.8004	0.0121	H-1→LUMO (66%), HOMO→L+1 (15%), HOMO→L+3 (10%)
	230.1587	0.0001	HOMO→LUMO (74%), HOMO→L+1 (15%)
$CHCl_3$	224.4870	0.0123	H-1→LUMO (65%), HOMO→LUMO (10%), HOMO→L+1 (14%)
	224.0084	0.0022	H-1→LUMO (22%), HOMO→L+1 (46%), HOMO→L+3 (15%)
Gas phase	234.6541	0.0014	HOMO→LUMO (83%), HOMO→LUMO (83%)
	231.5644	0.0044	H-1→LUMO (85%), H-1→L+2 (3%), HOMO→L+1 (6%)
	230.3683	0.0006	HOMO→L+1 (56%), H-1→LUMO (7%), H-1→L+1 (5%), HOMO→LUMO (7%), HOMO→L+2 (7%), HOMO→L+3 (6%), HOMO→L+4 (6%), HOMO→L+5 (2%)

but another bathochromic shift from $CHCl_3$ results. From the above results, it is very convincing that polarity plays a major role in contributing to the shift in the electronic spectra. The major transitions are of the type $\pi \rightarrow \pi^*$ which is caused by the two double bonds.

HOMO-LUMO analysis

Among the most important characteristics that affect the chemical stability of a molecule are the Frontier molecular orbitals (FMOs) and the interactions between the atoms. Such features are effective for judging optical and biological activities. Among the most important FMO's are the highest occupied molecular orbital (HOMO) that shows the ability to donate an electron, and the lowest unoccupied molecular orbital (LUMO), which reflects the ability to accept an electron. Fig. S3 (Supplementary Information)reveals the electron density of the highest five occupied and lowest five unoccupied molecular orbitals. In the title compound, the HOMO, LUMO, and LUMO+1 orbitals were mostly localized over the two double bonds suggesting the major transitions are π-π^* as can be seen also in Table IV for the major orbital contribution of the first two lines in an electronic transition. HOMO-2 and LUMO+2 electron densities are observed to be localized on the oxygen atom of the ether functional group (O1). HOMO-1 has the electron density localized on the neighborhood of oxygen atom O1. In HOMO-3 and LUMO+3 the high electron density is shown around oxygen atom of the

alcohol (O2) atoms. LUMO+4 the electron density is localized over the two oxygen atoms. HOMO-4 has the electron distributed on the isopropyl group.

The energy gap between the HOMO and LUMO is considered to be important in predicting the major electronic transition. The values of the energy gaps (in eV) are estimated as; 5.91 for gas phase, 6.05 for $CHCl_3$, 6.11 for CH_3CN, 6.11 for MeOH and 6.12 for DMSO. This order is relatively in good agreement with the previous section of the absorption wavelength order and at the same time the order increasing polarities. The solvent of the highest polarity (DMSO) makes the largest energy gap (Fig. S4). (Supplementary Information).

Molecular electrostatic potential

The chemical reactivity of a given compound can be predicted by studying the MEP (molecular electrostatic potential). Through MEP it is possible to specify the sites in the molecule that are vulnerable for nucleophilic or electrophilic attacks. Also, we can identify the hydrogen-bonding interactions and better recognizing the possible biological processes.

The electronic surface potential of the optimized structure of sarcotrocheliol**1** is drawn in Figure 4.

One clear positive region, blue color, is concentrated over the H of the hydroxyl group (O*H*). This hydrogen atom is considered to have the highest electrophilic reactivity in the molecule. Two negative regions (red color) are found localized over the two oxygen atoms. These two positions have a relatively nucleophilic reactivity. The intermolecular hydrogen bonding is included in the MEP map.

Pharmacokinetic and molecular docking study

Physicochemical study

Table V displays (*vide supra*) the physicochemical parameters of the compound among reference drugs by applying different drug rules and filters. The isolated compound that meets with the criteria of the rules displaying the drug-like character. The rules include the molecular weight and number of rotatable bonds. When the molecular weight of the compound is less than 500, it is predicted that this compound can be easily moved, diffused and absorbed. Also, when the number of rotatable bonds in the compound is less than 10 it indicates that molecular flexibility is low. TPSA, which is correlated with the hydrogen bonding of a molecule, is considered to be an indicator of the bioavailability of the drug molecule, which can be identified by the Osiris tool based on the summation of surface contributors of polar fragments[27].

Toxicity potential

Table VI and Table VII represent the toxicity potential evaluation data of the compound as calculated by OSIRIS Property[27] and PreADMET Explorers[28], respectively. The software can expect the toxicity potential in its database based on the similarity of the studied drugs with known structures. The computational toxicity risk assessment is required to avoid any improper effect or when further drug screening is important[29].

Table V — Drug-likeness calculations of metal complexes based on Osiris property explorer

Property	value	Score
cLogP	5.876	0.359
logS	-4.085	0.714
M.wt	306	0.911
Drug-likeness	-4.823	0.007
Number of HBA:	2	
Number of HBD:	1	
MolPSA	23.37 A2	
MolVol	396.78 A3	
Drug overall score	0.168	

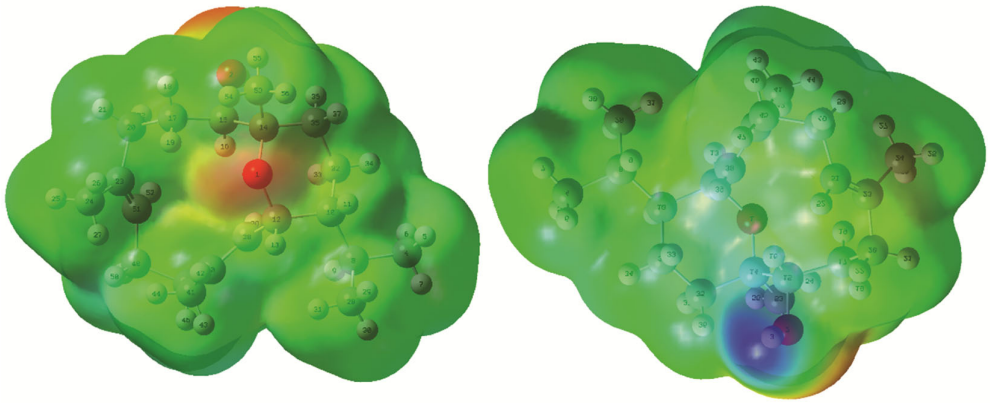

Figure 4 — The map's color code reflects the range from -6.21×10^{-2} eV (deepest red) to 6.21×10^{-2} eV (deepest blue)

Bioactivity score prediction

The bioactivity scores for a moderately active compound is expected to be from -5.0 to 0.0, whereas, higher than zero means a significant bioactive compound and less than -5 means the compound is inactive[30]. Sarcotrocheliol**1** has a score of 0.168 which suggests that our compound poses a considerable biological activities.

Table VI — Toxicity calculations of pyran-based cembranoids, sarcotrocheliol**1** based on Osiris property explorer

Toxicity	score	Type of risk
Mutagenicity	1	No risk
Tumorgenicity	1	No risk
Irritating effects	0.6	High risk
Reproductive effects	1	No risk

Table VII — Toxicity calculations of the compound based on PreADMET property explorer

Toxicity	Value
Acute algae toxicity	0.00865068
Ames test*	non-mutagen
Bioassay on carcinogenicity in mouse for 2 years	positive
Bioassay on carcinogenicity in rat for 2 years	negative
Acute daphina toxicity	0.0915107
in vitro Human ether-a-go-go related gene channel inhibition	Low risk
Acute fish toxicity (medaka)	0.0110459
Acute fish toxicity (minnow)	0.00116672
In vitro Ames test results for strain TA100 (Metabolic activation by rat homogeneous liver)	negative
in vitro Ames test results for strain TA100 (No metabolic activation)	negative
in vitro Ames test results in TA1535 strain (Metabolic activation by rat liver homogenate)	negative
in vitro Ames test results in TA1535 strain (Metabolic activation by rat liver homogenate)	negative

* Ames test is used for the examination of mutagenicity of a compound[32].

Pharmacokinetic parameters and toxicity potential by Molinspiration

Another method to determine the bioactivity score is by Molinspiration, especially for drug target compounds (Table VIII). As the value gets higher than zero the compound's activity increases whereas the value of fewer than zero means inactive (typically -0.5 to 0.0). Any value that is less than -0.5 corresponds to an inactive compound[31]. The results of sarcotrocheliol**1** showed some significant drug-likeness activity against nuclear receptor ligands and enzyme inhibitor whereas it shows moderate activity toward GPC ligand, ion channel and protease inhibitor. On the other hand, the compound reveals inactivity against Kinase inhibitor. We beleive that the differences in bioactivity correlate to the changes in the compound-protein interactions.

Molecular docking study

The molecular docking score between sarcotrocheliol **1** compound with PDB code = 1hk7 (breast cancer protein) and PDB code = 2q7k (prostate cancer protein) were estimated as -6.31 and -5.92, respectively. The study was done using the MOE program. The results reveal a good docking score for the compound toward both proteins with a relatively higher score toward 2q7k. This can be explained by the interaction mode of the compounds toward the proteins cancer from the oxygen of oxabicyclo to Val(365) amino acid of prostate cancer by hydrogen donor hydrogen acceptor interaction as described in Figure 5 and Figure 6 [23,24].

Table VIII — Bioactivity score of the compounds

Molinspiration bioactivity score v2018.03	
GPCR ligand	0.20
Ion channel modulator	0.27
Kinase inhibitor	-0.45
Nuclear receptor ligand	0.69
Protease inhibitor	0.19
Enzyme inhibitor	0.59

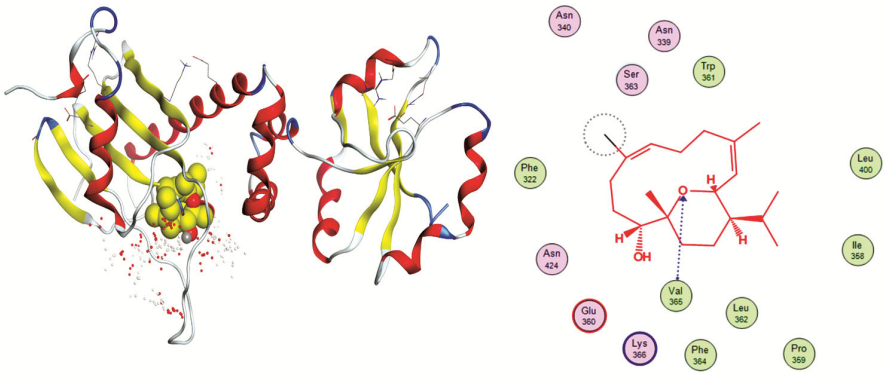

Figure 5 — 3D and 2D docking interaction of the isolated compound with breast cancer protein (PDB code = 1hk7)

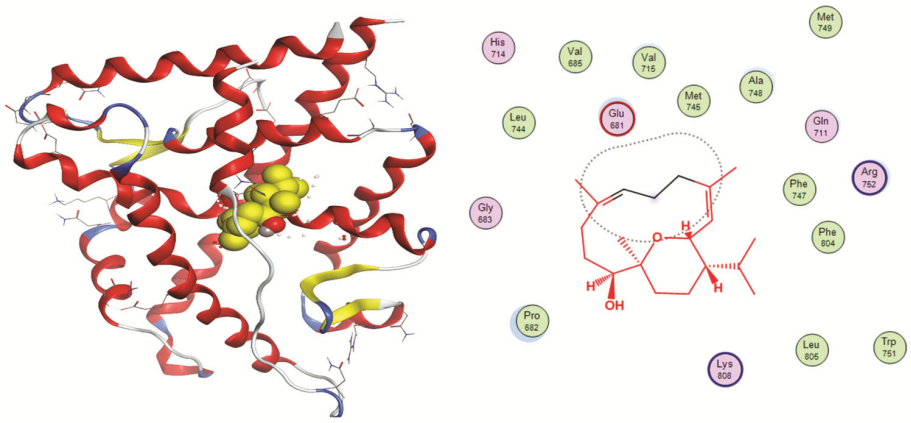

Figure 6 — 3D and 2D docking interaction of the isolated compound with prostate cancer protein (PDB code = 2q7k)

Conclusions

A recently discovered rare marine origin cembranoid compound was studied experimentally and theoretically to determine its structural and electronic information. Single crystal X-ray method was used to obtain the exact sarcotrocheliol 1 crystal structure showing that the molecule is crystalline as a $P2_12_12_1$ space group orthorhombic. Experimentally and theoretically, ^1H, ^{13}C and DEPT-135 NMR spectra of 1 were measured in four different solvents; $CDCl_3$, DMSO-d_6, MeOH-d_4 and CD_3CN. Density functional theory (DFT) approach has been used for computational properties at the theory level B3LYP/6-311++G(d, p). A comparatively good agreement between the experimental values with the theoretical vibrational frequencies calculated by DFT calculations. Time-dependent DFT (TD-DFT) implanted with the polarizable continuum model (PCM) was used to calculate the electronic absorption spectra in the gas phase and in the specified solvents. The correlation coefficients between the calculated (DFT/GIAO) and experimental NMR chemical shifts are found to be 0.92 and 0.998 for ^1H and ^{13}C NMR, respectively. The compound shows a significant activity toward prostate cancer and breast cancer protein. It also appears to have lower toxicity toward TA100 and TA1535 strains.

Supplementary Information

Supplementary information is available in the website http://nopr.niscair.res.in/handle/123456789/58776.

Conflict of Interest

The authors declare that there is no conflict of interest regarding the publication of this article.

References

1 Faulkner D J, *Nat Prod Rep*, 19(1) (2002) 1. http://dx.doi.org/10.1039/b009029h

2 Rodríguez A D, *Tetrahedron*, 51(16) (1995) 4571. http://dx.doi.org/http://dx.doi.org/10.1016/0040-4020(95)00216-U

3 Bernardelli P & Paquette L A, *Heterocycles*, 49 (1998) 531.

4 Coll J C, *Chem Rev*, 92(4) (1992) 613. http://dx.doi.org/10.1021/cr00012a006

5 Kamel H N & Slattery M, *Pharmaceutical Biology*, 43(3) (2005) 253. http://dx.doi.org/10.1080/13880200590928852

6 Li Y & Pattenden G, *Nat Prod Rep*, 28(7) (2011) 1269. http://dx.doi.org/10.1039/C1NP00023C

7 Lu Y, Huang C Y, Lin Y F, Wen Z H, Su J H, Kuo Y H, Chiang M Y & Sheu J H, *J Nat Prod*, 71(10) (2008) 1754. http://dx.doi.org/10.1021/np8003563

8 Chao C H, Wen Z H, Wu Y C, Yeh H C & Sheu J H, *J Nat Prod*, 71(11) (2008) 1819. http://dx.doi.org/10.1021/np8004584

9 Vinothkumar S & Parameswaran P S, *Biotechnology Advances*, 31(8) (2013) 1826. http://dx.doi.org/10.1016/j.biotechadv.2013.02.006

10 Al-Footy K O, Alarif W M, Asiri F, Aly M M & Ayyad S-E N, *Med Chem Res*, 24 (2) (2015) 505. http://dx.doi.org/10.1007/s00044-014-1147-1

11 Sheldrick G, *Acta Crystallogr Sect A*, 64(1) (2008) 112. http://dx.doi.org/doi:10.1107/S0108767307043930

12 Sheldrick G M, University of Gottingen, Germany (1997).

13 Macrae C F, Edgington P R, Mccabe P, Pidcock E, Shields G P, Taylor R, Towler M & Van De Streek J, *J Appl Crystallogr*, 39(3) (2006) 453. http://dx.doi.org/doi:10.1107/S002188980600731X

14 Frisch M J, Trucks G W, Schlegel H B, Scuseria G E, Robb M A, Cheeseman J R, Scalmani G, Barone V, Mennucci B, Petersson G A, Nakatsuji H, Caricato M, Li X, Hratchian H P, Izmaylov A F, Bloino J, Zheng G, Sonnenberg J L, Hada M, Ehara M, Toyota K, Fukuda R, Hasegawa J, Ishida M, Nakajima T, Honda Y, Kitao O, Nakai H, Vreven T, Montgomery J A, Peralta J E, Ogliaro F, Bearpark M, Heyd J J, Brothers E, Kudin K N, Staroverov V N, Kobayashi R, Normand J, Raghavachari K, Rendell A, Burant J C, Iyengar S S, Tomasi J, Cossi M, Rega N, Millam J M, Klene M, Knox J E, Cross J B, Bakken V, Adamo C,

Jaramillo J, Gomperts R, Stratmann R E, Yazyev O, Austin A J, Cammi R, Pomelli C, Ochterski J W, Martin R L, Morokuma K, Zakrzewski V G, Voth G A, Salvador P, Dannenberg J J, Dapprich S, Daniels A D, Farkas, Foresman J B, Ortiz J V, Cioslowski J & Fox D J, *Journal*, (Issue) (2009). http://dx.doi.org/citeulike-article-id:9096580

15 Software C.

16 O'boyle N M, Tenderholt A L & Langner K M, *J Comput Chem*, 29(5) (2008) 839. http://dx.doi.org/10.1002/jcc.20823

17 Jamroz M H, *Vibrational Energy Distribution Analysis Veda 4* (Warsaw) 2004-2010.

18 Khan T, Azad I, Ahmad R, Raza S, Dixit S, Joshi S & Khan A R, *Excli Journal*, 17 (2018) 331. http://dx.doi.org/10.17179/excli2017-984

19 Meyer P, Prodromou C, Hu B, Vaughan C, Roe S M, Panaretou B, Piper P W & Pearl L H, *Molecular Cell*, 11(3) (2003) 647. http://dx.doi.org/10.1016/s1097-2765(03)00065-0

20 Askew E B, Gampe R T, Stanley T B, Faggart J L & Wilson E M, *J Biol Chem*, 282(35) (2007) 25801. http://dx.doi.org/10.1074/jbc.M703268200

21 Al-Khathami N D, Al-Rashdi K S, Babgi B A, Hussien M A, Nadeem Arshad M, Eltayeb N E, Elsilk S E, Lasri J, Basaleh A S & Al-Jahdali M, *J Saudi Chem Soc* (2019). http://dx.doi.org/https://doi.org/10.1016/j.jscs.2019.03.004

22 Mashat K H, Babgi B A, Hussien M A, Nadeem Arshad M & Abdellattif M H, *Polyhedron*, 158 (2019) 164. http://dx.doi.org/https://doi.org/10.1016/j.poly.2018.10.062

23 Abdellattif M H, Hussien M A & Alzahrani E, *Int J Pharm Sci Res*, 9(12) (2018) 5060. http://dx.doi.org/10.13040/ijpsr.0975-8232.9(12).5060-78

24 Abdel-Rhman M H, Hussien M A, Mahmoud H M & Hosny N M, *J Mol Struct*, 1196 (2019) 417. http://dx.doi.org/10.1016/j.molstruc.2019.06.092

25 Al-Otaibi J S, *Tautomerization, Molecular Structure, Transition State Structure, and Vibrational Spectra of 2-Aminopyridines*: *A Combined Computational and Experimental Study*SpringerPlus [Online], p. 586 (2015). PubMed. http://europepmc.org/abstract/MED/26543721 http://europepmc.org/articles/PMC4628003?pdf=render http://europepmc.org/articles/PMC4628003 http://dx.doi.org/10.1186/s40064-015-1363-2 (accessed 2015).

26 Andersson M P & Uvdal P, *J Phys Chem A*, 109(12) (2005) 2937. http://dx.doi.org/10.1021/jp045733a

27 Ertl P, Rohde B & Selzer P, *J Med Chem*, 43(20) (2000) 3714. http://dx.doi.org/10.1021/jm000942e

28 Lee S, Lee I, Kim H, Chang G, Chung J & No K, *EuroQSAR 2002 Designing Drugs and Crop Protectants*: *Processes*, *problems and solutions*, 2003 (2003) 418.

29 Bala N, Raj J & Kandakatla N, *Int J Pharm Pharm Sci*, 7 (2015) 295.

30 Verma A, *Asian Pacific J Tropical Biomedicine*, 2, (3, Supplement) (2012) S1735. http://dx.doi.org/https://doi.org/10.1016/S2221-1691(12)60486-9

31 Sander T, *Gewerbestrasse*, 16 (2010) 4123.

32 Ames B N, Gurney E G, Miller J A & Bartsch H, *Proc Natl Acad Sci* (*USA*), 69(11) (1972) 3128. http://dx.doi.org/10.1073/pnas.69.11.3128